ELSEVIER

Sensors and Actuators A 52 (1996) 216–220

SENSORS AND ACTUATORS A PHYSICAL

Dynamics of polysilicon parallel-plate electrostatic actuators

Patrick B. Chu, Phyllis R. Nelson, Mark L. Tachiki, Kristofer S.J. Pister

Department of Electrical Engineering, University of California at Los Angeles. 405 Hilgard Avenue, Los Angeles, CA 90095-1594, USA

Abstract

The response of a polysilicon parallel-plate electrostatic actuator to a.c. signals at different bias voltages has been measured with a laser interferometer. Using microhinges, large plates (with areas from 100 μm^2 to ≈ 0.1 mm^2) with long thin support beams (such as 600 $\mu m \times 3$ $\mu m \times 1.5$ μm) are rotated off the surface of the substrate to form a parallel-plate capacitor. Fabricated structures having 100 μm gaps can be closed electrostatically with voltages as low as 50 V. This new actuator is estimated to output a force of up to 50 μN. With the exception of the resonant Q-value, the experimental results are in good agreement with simulations based on a simple nonlinear model for the actuator.

Keywords: Parallel-plate electrostatic actuator; Nonlinear dynamics; Squeeze-film damping; Polysilicon microgripper; Optical measurement; Surface micromachining

1. Introduction

Electrostatic actuation is used in many microelectromechanical systems due to its simplicity of operation, ease of fabrication and large force output. Many electrostatic actuators and microgrippers have been demonstrated. However, because of geometry limitations, these actuators generally have small areas for capacitor surfaces, resulting in limited force and displacement output. Furthermore, the motion of the actuators often takes place on or near the surface of the substrate so that it is difficult to use these actuators to create actuation far away from the substrate.

Using microhinges, three-dimensional polysilicon structures with high resolution in planar and vertical directions have been demonstrated previously [1]. The micro-actuator design described in this paper uses a similar commercial surface-micromachining process [3] to create large parallel plates to form a capacitor. Since the fabrication process puts a minimum constraint on the area of the plates and the length and width of the support beams, the actuator can be designed to operate over a relatively large range of forces and distances.

Predicting the dynamics of the parallel-plate actuators is difficult since both electrostatic actuation and squeeze-film damping are inherently nonlinear. Testing of the microstructure is also challenging, since the commercial process does not easily allow sensing elements to be incorporated into the structure. In the following sections, the design of the different components of the parallel-plate electrostatic actuator will be discussed. Modeling and testing issues will also be addressed. Then preliminary data will be presented.

2. Design and theory

Fig. 1 shows a design of a parallel-plate electrostatic actuator. The actuator has two large plates suspended by long thin beams which are connected to two support plates. Each half of the actuator is rotated to a vertical position from the substrate using microhinges. The support plates are locked into place by torsional spring locks (Fig. 2). To ensure that each side of the actuator remains perpendicular to the substrate, an addition locking plate with a slit holds the support plate from one side (Fig. 2 and Fig. 3). Long torsional polysilicon beams are used to create the electrical connection between the bonding pads on the substrate and the rotated plates (Fig. 3).

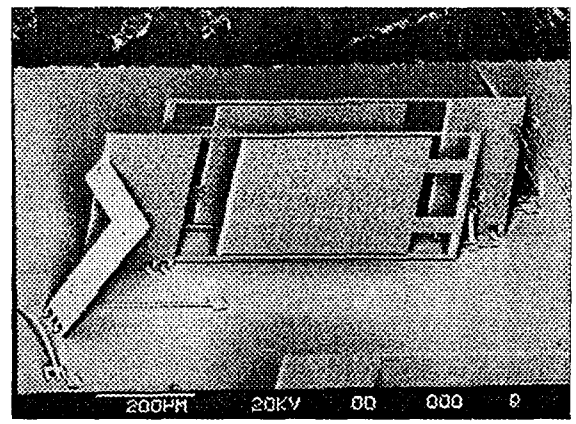

Fig. 1. A polysilicon parallel-plate electrostatic actuator.

SSDI 0924-4247(96)01116-8

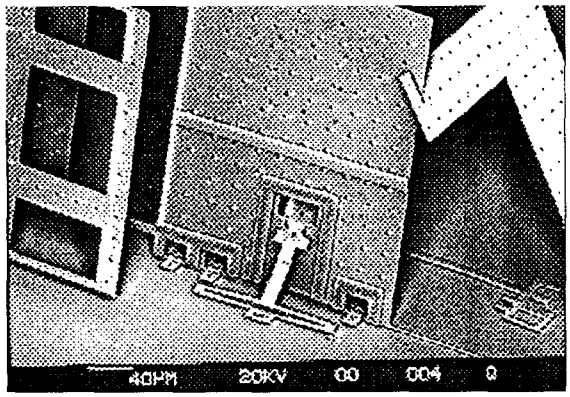

Fig. 2. A support plate of the actuator is locked in place with a torsional spring lock and a locking plate.

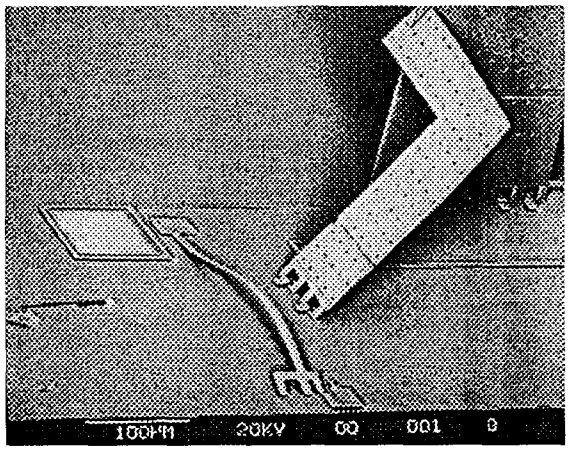

Fig. 3. A microjack is resting on the substrate in a buckled shape. The microjack dramatically simplifies the assembly process and thus increases the yield.

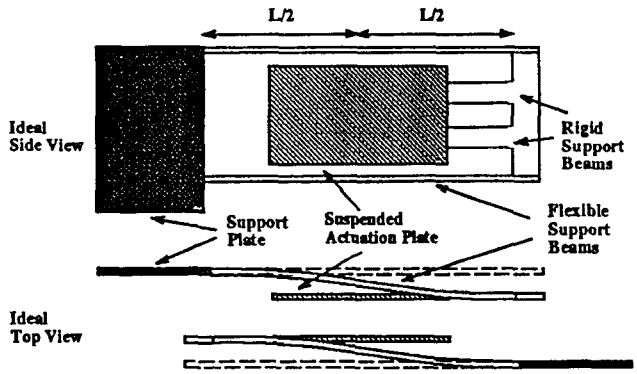

Fig. 4. Ideal top and side views of the suspended plates and support beams when a voltage is applied between the plates. The beam support is designed to provide parallel-plate deflection.

The two actuation plates remain parallel to each other due to a special support-beam design. The support beams and the suspended plates are connected in a folded configuration in order to eliminate the moment at the center of the beams and the derivatives at the ends of the beams. Fig. 4 shows the ideal curvature of the beams as the suspended plates move toward each other. When a voltage is applied between the two sides of the structure, an electrostatic attractive force decreases the gap between the suspended plates, thus bending the flexible support beams as shown.

The actuator is modeled as a parallel-plate capacitor. This assumption has been verified optically by determining the change in the angle of reflection from one actuator plate as a function of d.c. bias voltage. Angular rotation is observable but small. Furthermore, the direction of rotation is not constant as the offset voltage increases. For offset voltages less than 45 V, the maximum observed angular deviation is 0.4°. Due to the symmetry of the structure and small angular deviation, the motions of the actuation plates can be assumed to be parallel.

A structure similar to the parallel-plate electrostatic actuator may have applications in optics as a miniature Fabry–Pérot interferometer. The basic actuator design in Fig. 1 can also be modified into a microgripper as shown in Fig. 5. The hinged support plates are anchored at the same end of the structure, and gripper arms are attached to the free end of the actuator, far above the substrate.

The electrostatic attraction force for a given voltage V applied to the suspended parallel plates with area A and gap d is given by

$$f_e = -\frac{1}{2}\epsilon V^2 \frac{A}{d^2} = -\frac{k_e}{d^2}V^2 \tag{1}$$

The spring force required to displace the tip of a rectangular beam of length l and cross-sectional area $a \times b$ by a distance x is given by

$$f_s = n\frac{Ea^3b}{4l^3}x = k_s x \tag{2}$$

where E is Young's modulus of the material. For each of the beams in Fig. 4, $n = 4$ because of the moment and derivative assumptions. An equilibrium position of the suspended plates is reached when the electrostatic force and the total spring force from the support beams are matched. Since the electrostatic force increases as the square of the reciprocal of the gap between the plates, while the spring forces from the

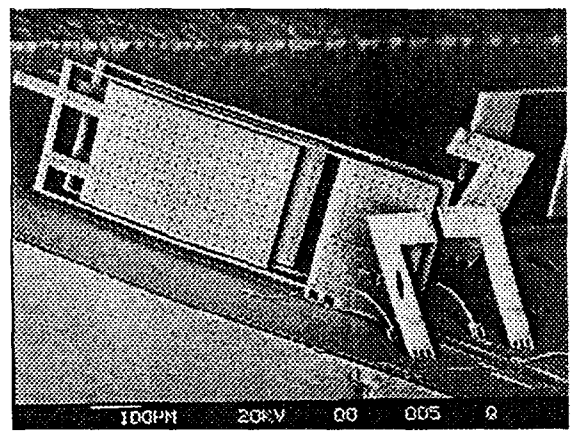

Fig. 5. A parallel-plate electrostatic actuator is configured to operate as a microgripper.

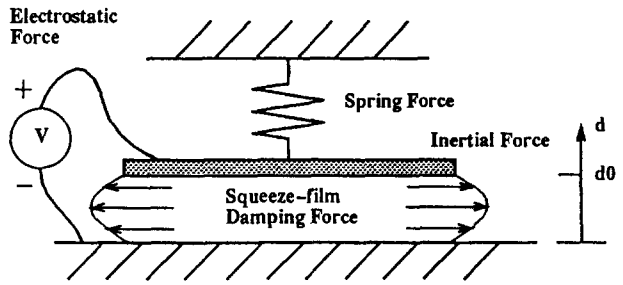

Fig. 6. Model of a parallel-plate electrostatic actuator. Forces are positive if they tend to increase the plate separation d.

flexible beams only increase proportionally to the deflection, only $d > d_0/3$ are stable equilibrium points.

Squeeze-film damping may be used to represent the damping experienced by the moving plates. Starr [2] presents the expression of this damping force for a rectangular plate of dimensions $2W \times 2L$ as

$$f_b = -\frac{16 c_{rect} W^3 L \mu}{d^3}\dot{d} = -\frac{k_b}{d^3}\dot{d} \tag{3}$$

where c_{rect} is approximately equal to

$$c_{rect} = 1 - 0.6\frac{W}{L} \qquad 0 < \frac{W}{L} < 1 \tag{4}$$

The model in Fig. 6 may be used to represent the parallel-plate electrostatic actuator including the inertia of the plates. The corresponding system equation is

$$2m_p\ddot{d} + \frac{k_b}{d^3}\dot{d} - 4k_s\left(\frac{d_0 - d}{2}\right) + \frac{k_e}{d^2}V^2 = 0 \tag{5}$$

where m_p is the mass of each suspended plate, d represents the gap distance between the two parallel plates, and d_0 is the initial gap (with no voltage applied). In the spring-force term, the additional factors of 4 and 1/2 are present since the actuator has four support beams, each of which is displaced by only half of $(d_0 - d)$.

3. Fabrication

Fabrication of basic three-dimensional structures using surface hinges has been described elsewhere [1]. Microactuators and microgrippers using the parallel-plate design with different dimensions and variations have been manufactured by MCNC [1], using three polysilicon layers (two are structural layers), two oxide layers, one metal layer, and one nitride layer in a seven-mask process. Post-processing is required to release and assemble the structures on the chips from MCNC. An acetone rinse and an RIE etch may be necessary if the chips have protective photoresist on the surface. A 49% HF etch and DI water rinse are required to remove the PSG sacrificial layers.

[1] MCNC Center for Microelectronic Systems Technologies, Research Triangle Park, NC 27709-2889, USA. Contact: Karen Markus.

Occasionally, microstructures with built-in locks are automatically assembled in the HF or DI water release rinse. Otherwise, the structures are assembled at a probe station, where a probe tip is placed underneath a selected plate and rotates the plate about its hinges. A buckled beam jack (or microjack), composed of a long flexible beam (about 300 μm $\times$ 10 μm $\times$ 2 μm in size) with one fixed end and an anchored catch, is used to raise the plate off the substrate to a height at which the probe tip can be placed underneath the plate easily (Fig. 3).

4. Experimental results

Several parallel-plate electrostatic microactuators have been tested open-loop with various d.c. and a.c. inputs, and the preliminary results are compared with computer simulation using Eq. 5. The data suggest that the model in Fig. 6 can provide reasonable predictions of the system's motion. The steady-state response of a similar actuator has been reported elsewhere[3].

In order to measure the dynamic response of the actuator, a Michelson interferometer was constructed in which the actuator plate of the test device is one of the mirrors, as shown in Fig. 7. The laser beam reflected by the moving microactuator is combined with part of the original laser beam to form an interference pattern, which is sampled by a photodiode. At a given d.c. offset, small-amplitude sinusoids, square waves, and impulses are applied to the system in order to determine its local behavior. Excitation input with small a.c. amplitudes is desirable because the resulting intensity change at the detector is much less than one fringe. As a result, by adjusting the second interferometer mirror, the detector signal can be made linearly proportional to the change of the plate position.

For a periodic symmetric sinusoidal input, the system outputs a periodic but slightly asymmetric waveform with the same frequency. The asymmetry indicates that the actuator experiences more damping when it closes than when it opens.

The simulated versus the actual frequency response of the actuator in Fig. 1 to a sinusoid with a p–p amplitude of 0.135 V at a d.c. offset of 12 V is shown in Fig. 8. The vertical scale indicates the simulated and actual p–p amplitudes of the peri-

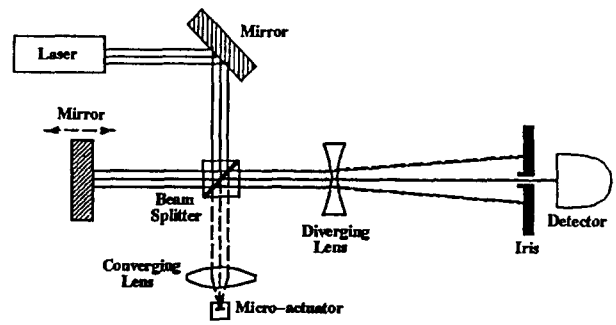

Fig. 7. The Michelson interferometer used to measure the deflection of the microactuator. One of the actuator plates is used as a mirror.

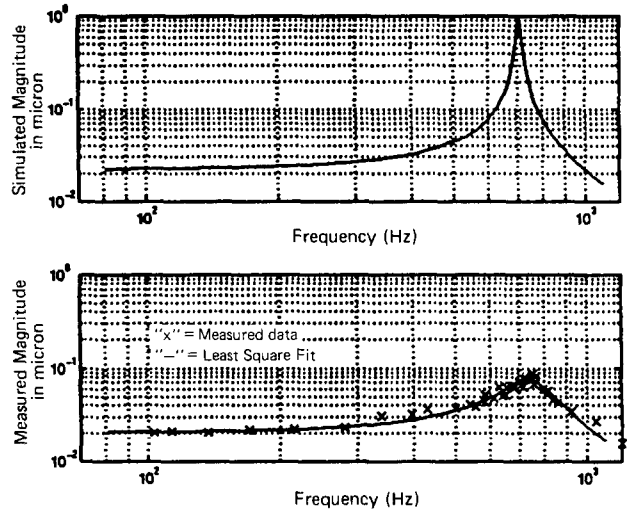

Fig. 8. Simulated and experimental Bode plots (small signal). The actuator in Fig. 1 is driven by 12 V d.c. and 135 mV sinusoid at different frequencies.

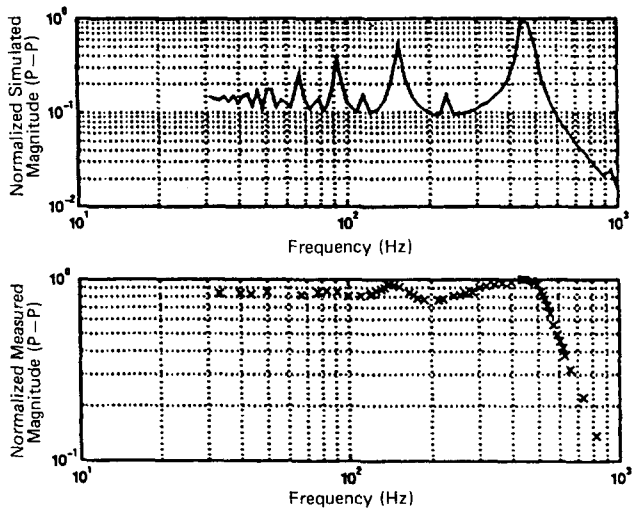

Fig. 9. Simulated and experimental Bode plots (large signal). An actuator similar to the one in Fig. 1 is driven by 10 V d.c. and 20 V square waves at different frequencies.

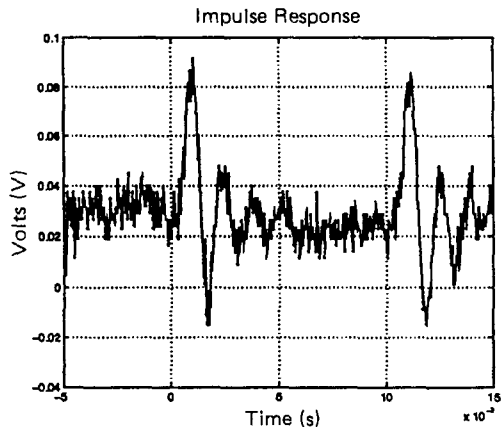

Fig. 10. Detector output when a 12 V d.c. and a 10 mV short pulse (700 μs) at 100 Hz are applied to the actuator.

odic output of the actuator in microns at different input frequencies. The simulation is performed using Matlab based on the nominal geometry of the design layout and published physical constants. This small-signal-amplitude plot resembles the frequency response of a linear mass–spring–damper system. The highest point of the experimental data occured at 750 Hz, while a least-square fit of the data predicts the resonance peak at 736 Hz. The resonance frequency from simulation using the model in Fig. 6 is 707.42 Hz. Although these two frequencies show reasonable agreement, the simulated quality factor is almost a factor of 12 higher than that of the curve fit.

The excellent agreement between the data and the simulation of the resonance indicates that the simple nonlinear model using typical values and parameters can provide sufficiently accurate predictions of the device. However, the discrepancy in quality factor suggests that the squeeze-film damping force is inadequate to represent all the damping experienced by the actuator.

When the a.c. and d.c. excitation amplitudes are increased significantly, multiple resonance peaks have also been observed in both simulations and experiments. Fig. 9 shows the frequency response of an actuator with only one moving side which is driven at a d.c. offset of 10 V and a square wave with a p–p amplitude of 20 V. Instead of using the Michelson interferometer, data are collected by detecting the horizontal angular change of the laser reflected by the actuator. The reflected laser is passed through an aperture to a photodiode detector. As a result, the measurement is not linear because the measurement system response saturates for large angular displacements. In this large-signal-amplitude plot the simulation predicted multiple resonances, which are present in the experiment results.

The Michelson interferometer was also used to study the actuator's responses to small impulses. Fig. 10 shows the detector output waveform when the actuator in Fig. 1 is given a d.c. offset of 12 V and is excited by 10 mV periodic pulses. From the damped oscillations after transitions, it was observed that the damped natural frequency f_d is about 730 Hz. The curve fit to the experimental data in Fig. 8 gives 743 Hz. This agreement suggests that the two methods of measuring the damped natural frequency using the interferometer provide very similar results. On the other hand, the simulation predicted a damped natural frequency of 707.46 Hz, which is only slightly higher than the predicted resonance frequency. This result again indicates that the actual system experiences more damping than is predicted in our model.

5. Conclusions

Large-displacement large-force polysilicon parallel-plate electrostatic actuators have been designed, fabricated, and tested. A laser interferometer in which the microactuator is used as a mirror provides accurate absolute measurement of the displacement dynamics of the microactuator. Experimen-

tal results and simulations generally agree, even though a relatively simple model was used. In order to characterize the system further and to improve our model of the system, we intend to test these devices in different gases and at different pressures.

References

[1] K.S.J. Pister, M.W. Judy, S. Burgett and R. Fearing, Microfabricated hinges, *Sensors and Actuators A, 33* (1992) 249–256.

[2] J.B. Starr, Squeeze-film damping in solid-state accelerometers, *Proc. IEEE Solid State Sensor and Actuator Workshop, Hilton Head Island, SC, USA, 4–7 June, 1990*, pp. 44–47.

[3] P.B. Chu and S.J. Pister, Analysis of closed-loop control of parallel-plate electrostatic microgrippers, *Proc. IEEE Int. Conf. Robotics and Automation, San Diego, CA, USA, 8–13 May, 1994*, pp. 820–850.

Biographies

Patrick B. Chu received his M.S. in electrical engineering from the University of California, Los Angeles, in 1994. He received his B.S. in electrical engineering from Massachusetts Institute of Technology in 1992. He is currently pursuing his Ph.D. in electrical engineering at the University of California, Los Angeles. His research interests include control theories, actuation, and sensors in MEMS.

Phyllis R. Nelson is a senior lecturer and research engineer with interests in optical metrology of MEMS devices, optical materials, solid-state lasers, and optical detectors. Before joining UCLA, Dr Nelson was a systems engineer at Hughes Aircraft, designed electro-optic systems and superconductive electronics at TRW, and studied the energy-transfer processes in solid-state laser materials at Université Claude Bernard-Lyon I in Lyon, France.

Mark L. Tachiki is working towards a bachelor's degree in electrical engineering from the University of California, Los Angeles. He has participated in research at the Department of Electrical Engineering at the University of California, Los Angeles, since 1994. His work includes automated CAD layout synthesis for MEMS and experimental measurement for MEMS.

Kristofer S.J. Pister is a part and product of the University of California. He received his Ph.D. and M.S. degrees in electrical engineering from Berkeley in 1992 and 1989, and his B.A. in applied physics from San Diego in 1986. Since 1992 he has been an assistant professor in the Electrical Engineering Department of the Los Angeles campus. His research interests include system design and CAD for MEMS and microrobotics.